Article:

Zhao, Yunjiang, Qiao, Gang, Liu, Songzuo et al. (2 more authors) (2020) Self-Interference Channel Modeling for In-Band Full-Duplex Underwater Acoustic Modem. Applied Acoustics. 107687. ISSN 0003-682X

https://doi.org/10.1016/j.apacoust.2020.107687

Self-Interference Channel Modeling for In-Band Full-Duplex Underwater Acoustic Modem

Yunjiang Zhao[a,b,c], Gang Qiao[a,b,c], Songzuo Liu[a,b,c,*], Yuriy Zakharov[d], Niaz Ahmed[a,b,c]

[a] *Acoustic Science and Technology Laboratory, Harbin Engineering University, Harbin 150001,China*
[b] *Key Laboratory of Marine Information Acquisition and Security (Harbin Engineering University), Ministry of Industry and Information Technology; Harbin 150001, China*
[c] *College of Underwater Acoustic Engineering, Harbin Engineering University, Harbin 150001, China*
[d] *Department of Electronic Engineering, University of York, U.K*

Abstract

In-band full-duplex (IBFD) underwater acoustic (UWA) communication can significantly improve the throughput of UWA communication networks. In this paper, we focus on the self-interference (SI) channel modeling which is essential for SI cancellation in an IBFD modem. The SI consists of direct self-loop interference (SLI) and self multi-path interference (SMI) due to reflections from water surface and bottom. Therefore, we first propose a simplified finite element model for SLI in an IBFD UWA modem. Then we model the underwater vertical channel to obtain the SMI path loss and propagation delays. Simulation results show that the SLI signal is composed of diffraction and scattering components, and it is greatly affected by the modem housing material and shape. The SLI channel has a long (several tens of ms) impulse response. To verify the proposed model, based on the IBFD UWA communication modem developed by our team, we conducted a lake experiment in December 2019 at Qiandao Lake in Hangzhou, China. The simulated results match well with the experimental results in time/frequency features and transmission loss. This study reveals the complexity of SI channel in IBFD UWA communication.

Keywords: Channel model, Full-duplex, Self-loop interference, Self-interference, Underwater acoustic communication.

1. Introduction

Underwater acoustic (UWA) communication technology has been widely studied and applied in many fields, such as underwater sensor networks, observation of marine environment, oceanographic engineering construction, etc. [1, 2]. Due to the narrow available frequency bandwidth and complex UWA propagation, the spectral efficiency of UWA communication systems is limited [3–5]. Full-duplex (FD) communication technology was introduced to improve the spectral efficiency of radio communication systems [6–8], and it can also be used for UWA communication systems.

A series of research work has been devoted to exploring the feasibility of FD technology in UWA communication systems [9, 10], especially the in-band full-duplex (IBFD) technology as it can double the utilization of frequency band and greatly improve the performance of UWA communication networks [11–16]. In general, the research has been focused on self-interference (SI) cancellation, which is the basis and major challenge of FD communications, and can be implemented as analog SI cancellation and digital SI cancellation. The performance of SI cancellation can be improved with more accurate estimates of the SI channel [11–13]. Therefore, it is of great significance to study the SI signal and SI propagation channel. In [13], a sparse adaptive constraint algorithm for estimation of the SI channel and power amplifier (PA) nonlinearity is proposed. An improved maximum likelihood (ML) algorithm for the SI channel estimation is proposed in [14], which introduces a penalty that favors sparsity in the cost function to obtain better SI channel

*Corresponding author
Email addresses: zhaoyunjiang@hrbeu.edu.cn (Yunjiang Zhao), qiaogang@hrbeu.edu.cn (Gang Qiao), liusongzuo@hotmail.com (Songzuo Liu), yury.zakharov@york.ac.uk (Yuriy Zakharov), ahmed@hrbeu.edu.cn (Niaz Ahmed)

estimates. In [11], the SI channel estimates are obtained by using the recursive least-squares (RLS) algorithm with dichotomous coordinate descent (DCD) iterations, which achieves 69 dB SI cancellation performance with the PA output being used as the regressor in the adaptive filter to deal with the non-linear distortions.

It should be noted that the SI signal between transducer and receiver is composed of self-loop interference (SLI) and other self-multi-path interference (SMI). The SLI component propagated through the modem housing is much stronger than the SMI component caused by reflections from the seabed and sea surface. A hybrid design proposed in [12] includes analog, digital cancellation and directional transmission. It can be used for the SLI cancellation in the deep ocean environment. Real sea measurements of SI for FD UWA communication systems are presented in [17], which demonstrate that the SMI can last more than 1 second in shallow water environments.

In practice, the SI cancellation algorithms will run in a communication modem like the one described in [9], so it is essential to consider the influence of the equipment (housing) on the SLI signal. The SMI channel can be modeled by combining some empirical formulas and models [3, 18]. In contrast, it is hard to describe and model the SLI channel realistically at sound propagation distances of only tens of centimeters. Furthermore, the SLI acoustic channel is different from the SLI in IBFD radio channel [19, 20]. The scattering component [21] caused by the IBFD UWA modem housing vibration will also be received by the near-end receiver in the form of interference. With a high transmission power, the far-end signal can not fit within the limited dynamic range of analog to digital converter (ADC). This requires an analog SI interference cancellation to enable the ADC to convert the far-end signal and further cancel the residual SI by a digital SI canceler [22]. Meanwhile, if some prior information about the SLI channel can be obtained, the complexity of analog interference cancellation can be reduced by digitally assisted analog interference cancellation [23]. Therefore, it is very important to model the SI channel, especially the SLI channel to obtain the prior information.

Hence, in order to better understand the SI channel in practice, especially characteristics of the SLI channel, such as the channel impulse response (CIR), in this work, we develop models for the SLI and SMI channels. First, to focus only on the SLI characteristics and channel modeling, the short distance sound propagation is simulated in infinite space without any interference from multipath components caused by boundaries. We establish a simplified finite element model of an IBFD UWA modem to simulate the sound propagation from the transmitter to the near-end receiver. Then we model the underwater vertical channel to obtain the SMI path loss and arrival time. The simulation results are verified in a lake experiment.

This paper is structured as follows: In section 2, we describe the modeling of SLI and SMI, the finite element model and parameter configuration. Analysis of the SLI signal is given in section 3. In section 4, the simulation results are verified by experiments. Finally, some conclusions and discussions concerning the use of IBFD UWA communication systems in practice are provided in section 5.

2. Modeling Method and Parameter Configuration

Normally, the conventional UWA communication modem can be roughly divided into two parts: the transceiver transducer and the housing. However, for the IBFD UWA communication modem, in order to transmit and receive signals at the same time, it is composed of three parts: transmitting transducer, receiving transducer and housing as shown in the left side of Fig. 1. The housing contains the digital, analog circuit boards and battery packs. The housing between the transmitting end and the receiving end will block the sound propagation path. Due to the complexity of the SLI propagation, it is difficult to obtain an analytical expression of the SLI channel model. Therefore, we use the finite element model of the IBFD UWA communication modem to simulate the propagation process. On this basis, we obtain characteristics of the SLI channel. For the SMI channel, we mainly calculate the arrival delay and attenuation of each path based on the spreading loss, absorption loss and reflection loss.

2.1. Simplified model of IBFD UWA communication modem

When the IBFD UWA communication modem transmits a signal through a transducer, the emitted sound wave will first interact with the housing. This interaction will produce an echo reflected by the housing and make the housing enter the vibration state causing the coupled vibrio-acoustics phenomenon. The housing under vibration will radiate elastic waves, which will be scattered into surrounding water and received by a receiving transducer.

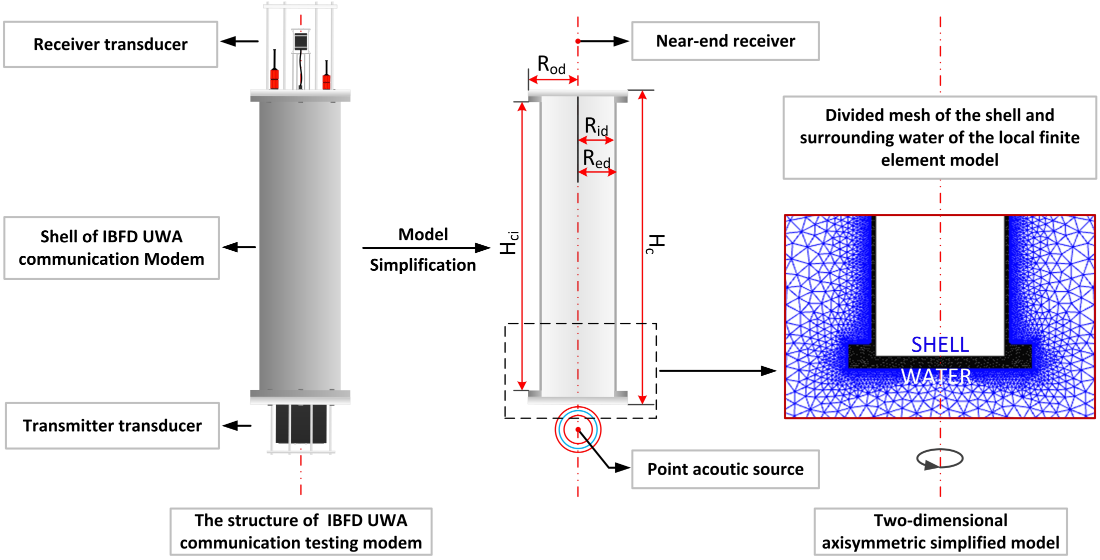

Figure 1: The simplified structure of IBFD UWA communication testing modem and its finite element model.

The above process can be represented as [24, 25]

$$\frac{1}{\rho_w c^2}\frac{\partial^2 p_t}{\partial t^2} - \frac{\nabla^2 p_t}{\rho_w} = \frac{4\pi}{\rho_w c} S(\delta(x)), \tag{1}$$

$$\rho_s \frac{\partial^2 u}{\partial t^2} = \nabla \cdot C_{au} + F_v, \tag{2}$$

where p_t is the total acoustic pressure, ρ_w and ρ_s are the density of the water and the housing respectively, c is the sound speed in water, S is the amplitude of monopole source, $\delta(x - x_0)$ is the unit-impulse function at coordinate x_0 , C_{au} is the Cauchy stress, u is the displacement vector as the inertia item and F_v is the volume force vector.

The numerical simulation of the coupling between acoustic wave and the housing is conducted by using a time-dependent solver in two-dimensional axisymmetric model. We use the coupling model of multi physical fields software COMSOL [26] to establish the boundary of acoustic-housing. As the perfect matching layer cannot completely eliminate the influence of the simulation space boundary, we simulate the vibro-acoustics coupling phenomenon in infinite space by setting the simulation space range far greater than the housing size, so as to ensure that there is no influence of the simulation boundary echo during the observation time. In this way, the simulation result in the observation time only contains the SLI, and there is no other interference.

In the finite element calculation, especially for the propagation problem in transient time, high time resolution is needed. Hence, we use the Courant-Friedrichs-Lewy (CFL) [27] and mesh size to calculate the time-step for controlling the simulation error. As we want to observe the short-range propagation, a smaller CFL is needed as it describes how many mesh elements can propagate per time-step.

The specific calculation process is as follows

$$\Delta t = \frac{CFL{\cdot}h}{c}, \tag{3}$$

where Δt is the time-step size, c is the sound velocity, and h is the mesh size. In this study, the frequency range of transmitted signal is 6-12 kHz, and CFL is set to 0.2. To ensure the accuracy of simulation, the maximum size of mesh elements of water and the housing-structure interface were about one-sixth and one-sixtieth of the minimum wavelength of transmitted signal, respectively. Due to the irregular shape of the housing, the model uses free triangle elements to deal with the irregular shape as shown on the right side of Fig. 1. The specific values of other parameters are shown in Table 1. The distance between the point sound source and the shell is 5 cm, while the distance between the receiving end and the shell is 10 cm as shown in fig. 1.

We use the broadband short-pulse transmitting signal in simulation. A window function is applied to

Table 1: Parameters of the simulation model.

Parameter	Value
Material	Aluminum 6063-T83
Transmitted signal	Broadband short-pulse signal S(t)
Water Density	1000 kg/m^3
Sound velocity in water	1500 m/s
R_{od}	105 mm
R_{id}	74 mm
R_{ed}	80 mm
H_c	530 mm
H_{ci}	500 mm

reduce the energy leakage and make it easier to identify the diffraction and scattering components in the experimental and simulation results [28].

The transmitted signal is given by

$$S(t) = A\cos\left[2\pi f_l t + \frac{\pi(f_h - f_l)t^2}{T_B}\right] \cdot W_H(t), (0 \le t < T_B), \tag{4}$$

where A is the amplitude of the transmitted signal, $W_H(t)$ is the Hamming window, T_B=0.5ms is the signal duration, $f_l = 6kHz$ and $f_h = 12kHz$. The transmitted signal and its spectrum before and after the windowing are shown in Fig. 2.

In this simplified model, we used a point source instead of the transducer transmitting sound waves. We also used a basic electroacoustic transducer model, but the results are almost the same. To reduce the computational complexity of the model further, we ignore the internal equipment of the housing and deal with it as air. Due to the large difference between the acoustic impedance of the air and housing, the air part can be further omitted. Note that it is difficult to extract the scattering waves and diffraction waves independently due to their heavy overlap in time. Therefore, to obtain the diffraction wave we set the housing to be absolutely rigid in an auxiliary simulation. In this auxiliary simulation, the configuration of other parameters was completely consistent with the above simulation parameters.

2.2. *Simplified model of vertical acoustic channel*

When the modem is working underwater, the near-end receiver will receive not only the SLI, but also the SMI. Compared with the far-end expected signal, this interference component cannot be ignored. To fully understand characteristics of the SMI channel, we consider arrival delay, spreading loss, absorption

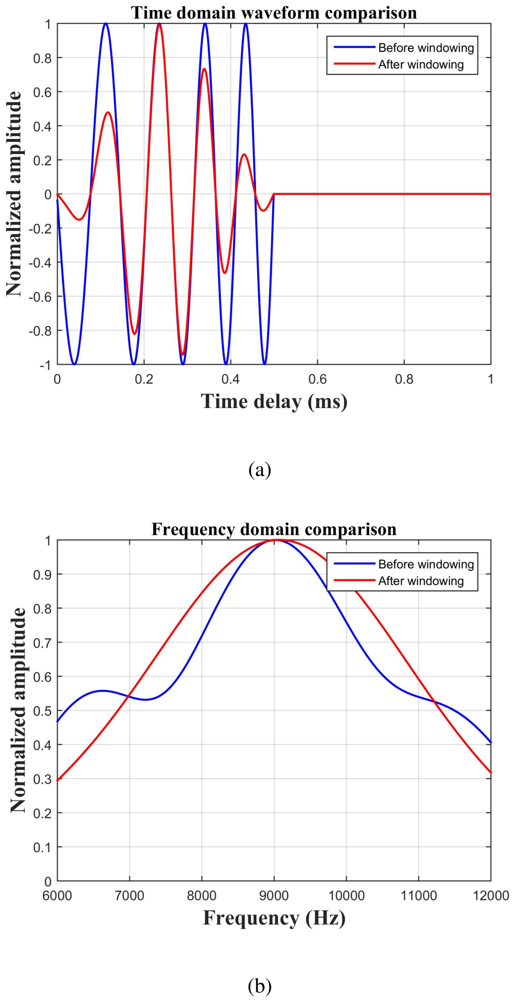

Figure 2: Comparison of signal before and after windowing: (a) Time domain; (b) Frequency domain.

loss and reflection loss to make a simple modeling of a vertical channel. For this model, the layout of the modem is shown in Fig. 3.

The modeling is based on a scenario in which the modem is placed vertically underwater. Considering two kinds of reflection, the blue line indicates that the first reflection is from the sea surface, and the red line indicates that the first reflection is from the sea bottom. The distances from the transducer and the receiver to sea surface are represented by D_t and D_r .The depth of the sea is expressed by D_p .

The arrival delay of reflections can be approximately computed as

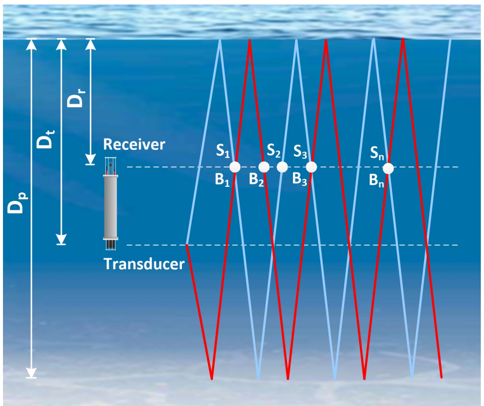

Figure 3: Reflections in a vertical channel.

$$T_{sn} = \frac{D_t + 2D_p \cdot \left\lfloor \frac{n}{2} \right\rfloor + D_r \cdot [2 \cdot (n \mod 2) - 1]}{c}, \quad (5)$$

$$T_{bn} = \frac{-D_t + 2D_p \cdot \left\lfloor \frac{n+1}{2} \right\rfloor - D_r \cdot [2 \cdot (n \mod 2) - 1]}{c}, \quad (6)$$

where T_{sn} is the arrival time after n reflections (for paths with the first reflection from the surface), T_{bn} is the arrival time after n reflections (for paths with the first reflection from the bottom), and c is the speed of sound. The spreading loss will increase with distance and can be obtained by the following formula [3]

$$S_{prd} = k \cdot 10 \cdot \log_{10}(l_d), \quad (7)$$

where S_{prd} is the spreading loss, k is the spreading factor taken to be 1.5 in this study, and l_d is the distance of propagation.

The absorption loss is a frequency-dependent function. Combined with the spreading loss, it can be expressed by the following formula [29]

$$A(l_d, f) = A_r {l_d}^k a(f)^{l_d}, \quad (8)$$

where A_r is a scale constant, $a(f)$ is the absorption factor, and it can be calculated by using the Thorps empirical formula [30]

$$a(f) = 0.11\frac{f^2}{1+f^2} + 44\frac{f^2}{4100+f^2} + 2.75 \times 10^{-4} f^2 + 0.003, \quad (9)$$

where f represents the transmitting signal frequency (in kHz).

For the reflection loss, we assume that the sea surface is flat and it can be modeled by a reflection coefficient $\gamma_s = -1$, and the bottom reflection loss R_{fb} and the bottom reflection coefficient γ_b can be expressed by [31]

$$R_{fb} = -20\log_{10}\left|\frac{p_r}{p_i}\right| = -20\log_{10}|\gamma_b|, \quad (10)$$

where p_r and p_i are the reflected and incident sound pressure amplitude, respectively. In this study, $\gamma_b = -0.97$ is adopted. Therefore, the overall path loss of the SMI can be represented in decibels by

$$PL_{all} = 10\log_{10}A(l_d, f) + \eta R_{fb}. \quad (11)$$

where η represents the number of times the path has reflected off the seafloor.

It should be noted that when the sea surface is calm, the coherence time of vertical acoustic channel is quite long. However, when the sea surface fluctuates due to wind and waves, the arrival time T_{sn} and T_{bn} in Eq.(5) and Eq.(6) will change with D_r, D_t and D_p. At the same time, due to the change of propagation time, the propagation distance l_d of each path will also change under the assumption of constant sound velocity. According to Eq.(7) and Eq.(8), the spreading loss and the absorption loss will also change. In addition, the sea surface fluctuations also affects the sea surface reflection coefficient γ_s, which will affect the overall path loss of the SMI. Therefore, the coherence time of shallow water acoustic vertical channel will be shorter. In practical applications, it is necessary to use the algorithm with certain adaptive processing ability to track the time-varying CIR of the SMI.

3. Analysis of simulation results

In this section, we use the simplified finite element model to simulate the sound propagation process and obtain the SLI at the near-end receiver. To investigate the influence of the housing on the SLI signal, we also simulate the short-range propagation without the housing for comparison.

3.1. Waveform analysis

Fig. 4 shows simulation results for the SLI signal in time and frequency domains. It can be seen in Fig. 4a and Fig. 4b that the received SLI waveform is quite different in the cases with and without the housing.

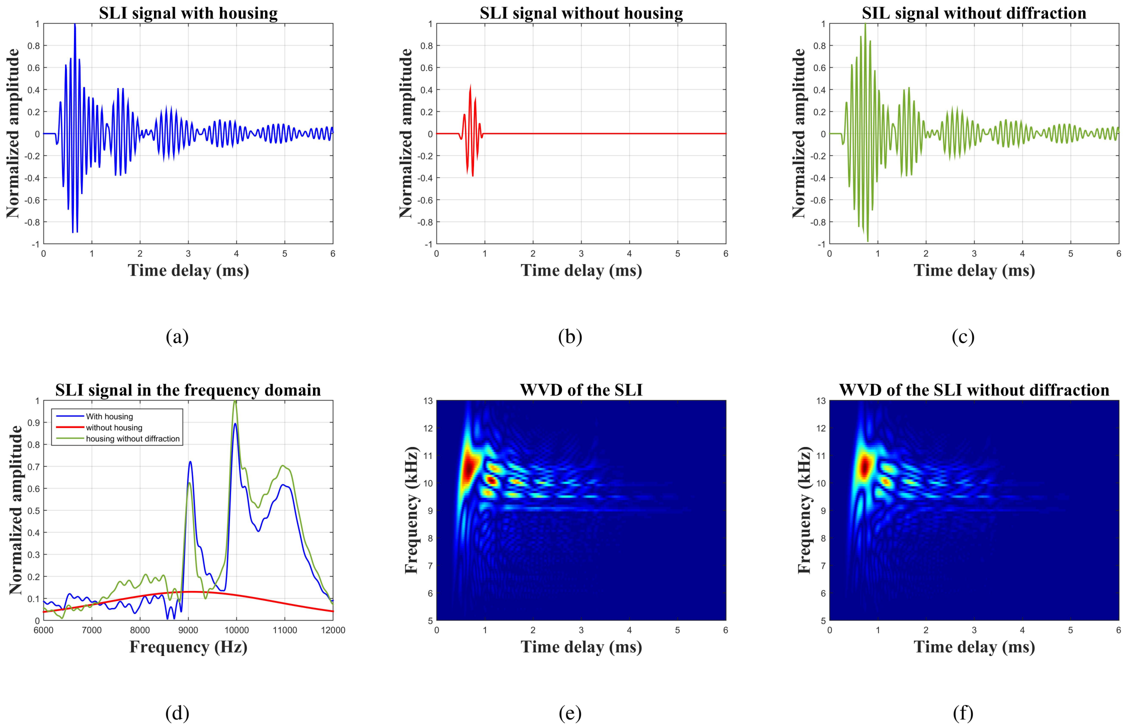

Figure 4: The SLI components. (a) Time domain. (b) Time domain (without housing). (c) Time domain (housing without diffraction). (d) Frequency domain. (e) WVD of the SLI signal. (f) WVD of the SLI signal without diffraction.

Amplitude with housing is significantly higher than that without it. This is due to the housing vibration and re-radiation. The complex form of the SLI signal is caused by the superposition of scattering and diffracted sound waves at the receiving point.

In addition, the peak amplitude of sound pressure before removing the housing is about twice that after removing the housing, that is to say, the existence of the housing increases the SLI by almost 6dB. The SLI signal without the diffraction is shown in Fig.4c. Fig.4d shows the SLI signal in the frequency domain. There are seen resonance peaks at about 9 kHz, 10 kHz and 11 kHz, which are defined by the housing material and its thickness. The SLI signal is equivalent to passing the transmitted signal through a frequency-selective channel, which needs to be considered in the SI cancellation process.

Fig.4e and Fig.4f show the time-frequency representations of the SLI signal before and after removal of the diffraction component. Here, we use the Wigner-Ville distribution (WVD) [32]. The difference between them is small, which shows that the main component of the SLI signal is the housing scattering component. In order to describe this process more

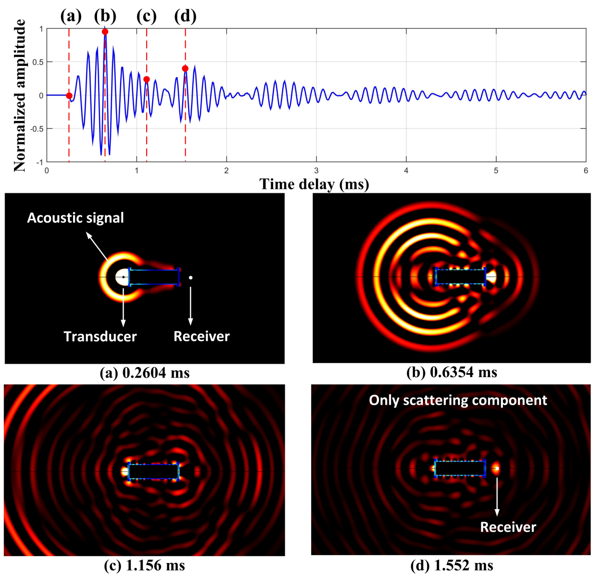

Figure 5: Snapshots of the propagation process: (a) 0.2604 ms; (b) 0.6354 ms; (c) 1.156 ms; (d) 1.552 ms.

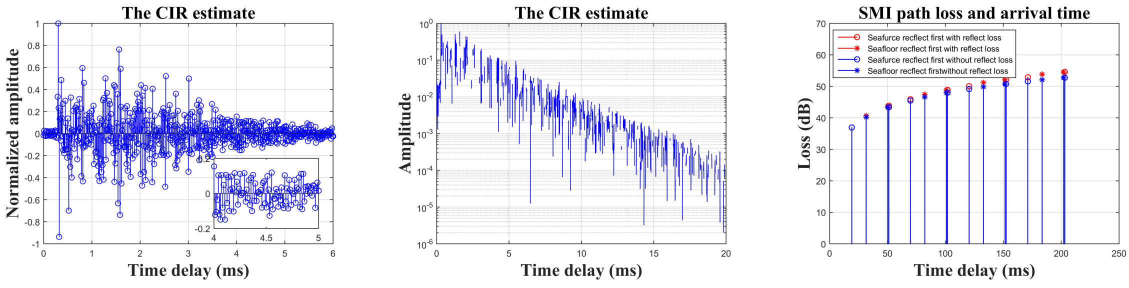

(a) (b) (c)

Figure 6: Channel simulation results. (a) The SLI channel within the first 6 ms. (b) The SLI channel estimate in logarithmic scale. (c) Path loss and arrival time of SMI channel taps.

clearly, Fig.5 shows snapshots of the SLI signal in space at different time instants.

As shown in Fig.5a that shortly after the acoustic signal is emitted from the transmitting transducer, the sound pressure changes at the near-end receiver, and the diffraction component has not yet reached there. At initial time period, the fluctuation of the sound pressure is caused by the sound scattering of the housing. At 0.6354 ms (see Fig.5b), the diffracted component arrives at the near-end receiver and overlaps with the scattering component. After the arrival of the diffraction component, the housing vibrates and radiates waves into the surrounding water. Fig.5d shows the subsequent scattering process, and only the scattering components remain in the simulation space.

3.2. CIR between the transducer and hydrophone

From the above analysis, it can be concluded that the SLI signal received by the near-end receiver contains diffraction and scattering components. We obtain the channel estimate in the process of the SLI propagation by using the recursive least-squares (RLS) algorithm. For the RLS algorithm, the forgetting factor is set to 0.998. The adaptive filter taps are the SLI channel estimate. The SLI CIR is shown in Fig.6a and Fig.6b, with different observation times. Fig.6a shows the complexity of the SLI channel for the first 6 ms, and it cannot be described as a sparse channel. From the simulation results, it can be seen that it is difficult to cancel the SLI by conventional SI interference cancellation just in analog domain, as the number of taps is too high. In Fig.6b, the 20 ms channel estimate is expressed in logarithmic scale. If we want to achieve certain interference cancellation effect, especially when it is more than 60dB, it means that the magnitudes of the adaptive filter taps that affect the SI performance could be as low as 10^{-3} to 10^{-4} with respect to the CIR maximum. Therefore, in practice, for the SI cancellation, the filter length should be set longer than 20ms.

3.3. SMI channel

We set here the simulation parameters similar to the one observed in the lake experiment. The distances from the transducer and the receiver to the sea surface are set to $D_t = 14.7\ m$ and $D_r = 14\ m$. The water depth is set to $D_p = 38\ m$ and the frequency is set to be 9 kHz as the center frequency of the test signal. The overall path loss and arrival time of the SMI are shown in Fig.6c. It can be seen that after multiple reflections, at 200ms, the energy of the SMI decreases by about 50dB, which is still very strong for the expected far-end signal. Such a long channel would be a substantial problem for the SI canceller.

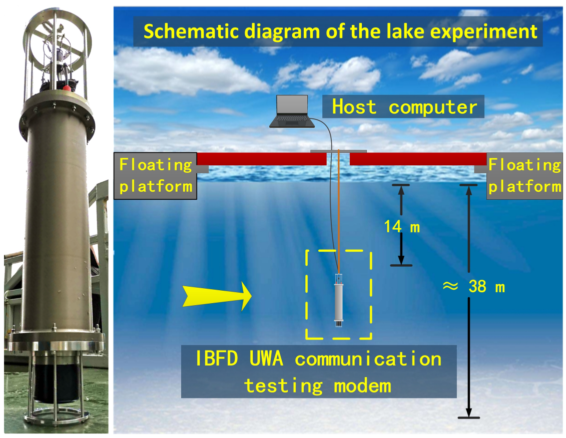

Figure 7: The lake experimental setup.

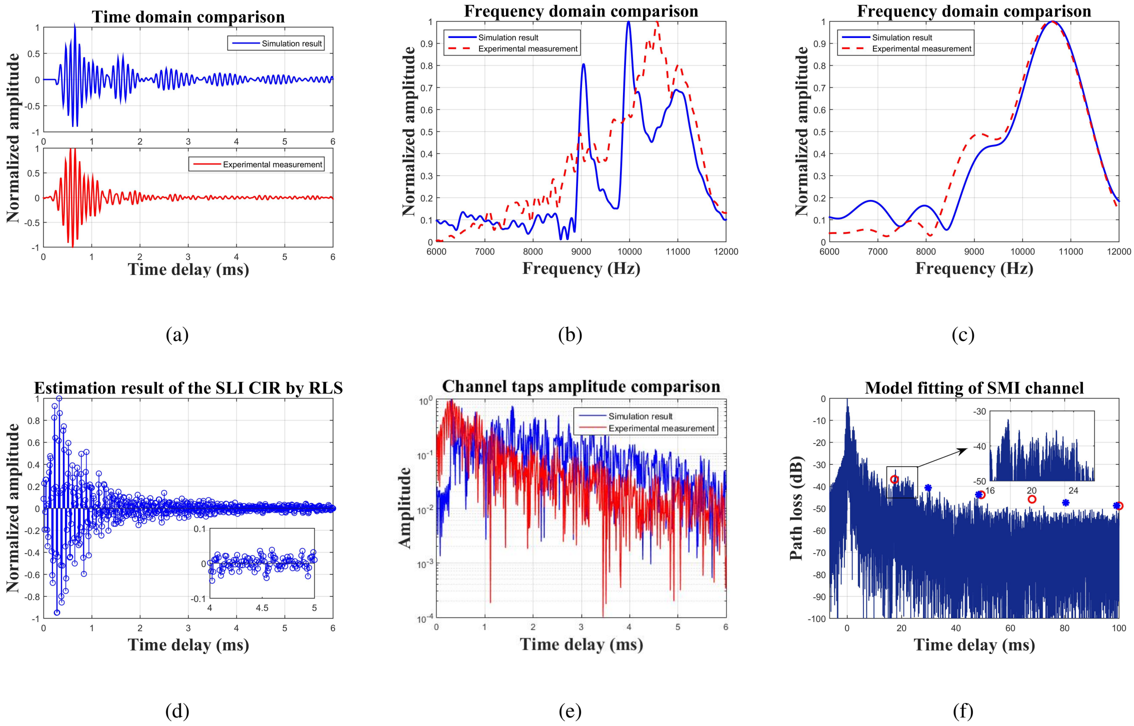

Figure 8: Comparison of simulation and measurement results. (a) Time domain. (b) Frequency domain. (c) Frequency domain comparison of the first 1.2 ms of the SLI signal. (d) Impulse response estimate with the measurement results. (e) Channel tap amplitude comparison. (f) The fitting of SMI channel model with the measurement results.

4. Lake experiment

The lake experimental setup is shown in Fig. 7. It was conducted in the Qiandao Lake, Hangzhou China. It was carried out on a large floating platform more than 100m away from the shore. The depth of the lake water is about 38 m. In order to verify the SLI and SMI channel, we put the hydrophone at a depth of 14 meters, so that the receiving end was not affected by the reflection of lake surface and bottom in a certain observation time (about 18 ms which is much longer than the duration of the transmitted signal).

4.1. Comparison of experimental and simulation

The test transmitting signal is the same as in the simulation. The comparison between the SLI signal received in the experiment and in the simulation is given in Fig. 8. It can be seen from Fig. 8a that the simulation of the first 1.2 ms is in good agreement with the measurement results, but after 1.2 ms, the scattering component of the SLI signal decays more rapidly in the practical measurement. The cross-correlation coefficient between the two signals was 0.94 for the first 1.2 ms and 0.79 for the first 6 ms.

The reason is that during the measurement, the housing was pulled by the rope, which is different from the state of the housing in the simulation. Under the action of the tensile force, the vibration of the housing decreases faster. Due to the lack of backscattering components, the fit of the SLI obtained by simulation and experiment is not high in frequency domain as shown in Fig. 8b. In contrast, as shown in Fig. 8c, the SLI of the first 1.2 ms has a better fit in the frequency domain, but there are still some differences due to the influence of the frequency responses of the transducer and the hydrophone. In Fig. 8d, the result of the SLI channel estimation in the lake experiment is plotted. Compared with the simulation result, it has faster decay but is also complex as shown in Fig. 8e. This may be due to the fact that in the actual measurement, due to the existence of the gravity of the housing and the tension on the tension rope, the vibration of the housing is restrained to a certain degree, which weakens the scattering process. These multi-path components cannot be ignored when compared to the expected far-end signal and need to be eliminated. The fit between the SMI channel model and the measurement is shown in Fig. 8f. Due to the difference between the bottom reflection coefficient setting and the real one, and other effects like non-frequency-flat transducer and hydrophone responses, there are several dB discrepancy between the simulation and measured values, but the overall trend is the same. In addition, it can be observed that there are a large number of small taps following the first path as shown in the enlarged figure in Fig. 8f, which is caused by the reflection of some housing scattering components from the surface to the near-end receiver. Therefore, the existence of the housing can also affect the SMI channel. In terms of the complexity of the SLI and SMI channel, in practice, we need to consider how to reduce the SLI component, e.g. by properly positioning the transducers.

5. Conclusions and discussions

In this study, we used a simplified finite element model of the IBFD UWA communication modem to simulate the influence of the housing on the SI at near-end receiver. The simulation results show that the SLI signal received by the near-end receiver contains diffraction component and scattering component, and the scattering component is more intensive. We also modeled the SMI channel and obtained the path loss and arrival time of different taps. The simulation results are verified in the lake experiment by using an IBFD UWA communication testing modem in December 2019. The experimental and simulation results showing the SLI waveform, its frequency spectrum and CIR of the SLI channel and the influence of housing on the SMI channel are given for the first time. It should be noted that when the IBFD UWA communication modem interacts with other nodes underwater, the duration of communication signal will be longer than the test signal used in this experiment. It means that the scattering components continuously generated by the housing will always be superposed with the transmitted signal at the near-end receiver. These effects make it difficult for SI cancellation.

In view of the simulation and experimental results, some discussions for the implementation of the IBFD UWA communication are given as follows:

- Compared with the case without the housing, the housing amplifies the SLI. Considering the good agreement between the simulation and experimental results, it can be inferred that in practice, the SLI will also increase under the influence of the housing. This makes us need to cancel a stronger SLI in the interference cancellation stage.

- Before the realization of the equipment, it is necessary to simulate the sound propagation process based on the housing structure and materials. We can reduce the influence of the scattering component on the SLI by changing the housing material and structure. For example, materials whose resonant frequencies do not coincide with the same frequency band may be selected for the housing. After the same excitation, housing materials with weak scattering components can be selected.

- More generally, the proposed SLI model can be useful for designing the modem housing and positioning the transducers with reduced self-interference.

6. Acknowledgements

This work was supported by the National Key R&D Program of China(Grant Nos. 2018YFC0308500), National Natural Science Foundation of China under (Grant Nos. 61771152, 11974090, 11774074 and 11704090), the Natural Science Foundation of Heilongjiang Province of China (Grant No. YQ2019F002). The Key Laboratory of Acoustic Environment, Institute of Acoustics, Chinese Academy of Sciences (Grant No. SHHJKFKT-1801) and Innovation Special Zone of National Defense Science and Technology.

The work of Y. Zakharov was partly supported by the UK EPSRC through the USMART (EP/P017975/1) and Full-Duplex (EP/R003297/1) projects.

The author wish to thank Xinyu Liu, Hanbo Jia, Shuyong Pang and others who participated in the lake experiment.

References

[1] J. Heidemann, M. Stojanovic, M. Zorzi, Underwater sensor networks: applications, advances and challenges, Philosophical Transactions of the Royal Society A: Mathematical, Physical and Engineering Sciences 370 (1958) (2012) 158–175, doi:10.1098/rsta.2011.0214.

[2] I. Akyildiz, D. Pompili, T. Melodia, Challenges for efficient communication in underwater acoustic sensor networks, ACM Sigbed Review 1 (2) (2004) 3–8, doi:10.1145/1121776.1121779.

[3] M. Stojanovic, J. Preisig, Underwater acoustic communication channels: Propagation models and statistical characterization, IEEE Communications Magazine 47 (1) (2009) 84–89, doi:10.1109/mcom.2009.4752682.

[4] M. C. Domingo, Overview of channel models for underwater wireless communication networks, Physical Communication 1 (3) (2008) 163–182, doi:10.1016/j.phycom.2008.09.001.

[5] D. E. Lucani, M. Stojanovic, M. Medard, On the relationship between transmission power and capacity of an underwater acoustic communication channel, in: OCEANS 2008 - MTS/IEEE Kobe Techno-Ocean, 1–6, doi:10.1109/OCEANSKOBE.2008.4531073, 2008.

[6] D. Bliss, P. Parker, A. Margetts, Simultaneous transmission and reception for improved wireless network performance, in: 2007 IEEE/SP 14th Workshop on Statistical Signal Processing, 478–482, doi:10.1109/SSP.2007.4301304, 2007.

[7] Z. Zhang, K. Long, A. V. Vasilakos, L. Hanzo, Full-duplex wireless communications: Challenges, solutions, and future research directions, Proceedings of the IEEE 104 (7) (2016) 1369–1409, doi:10.1109/JPROC.2015.2497203.

[8] K. E. Kolodziej, B. T. Perry, J. S. Herd, In-band full-duplex technology: Techniques and systems survey, IEEE Transactions on Microwave Theory and Techniques 67 (7) (2019) 3025–3041, doi:10.1109/TMTT.2019.2896561.

[9] G. Qiao, S. Liu, Z. Sun, F. Zhou, Full-duplex, multi-user and parameter reconfigurable underwater acoustic communication modem, in: 2013 OCEANS-San Diego, 1–8, doi:10.23919/OCEANS.2013.6741096, 2013.

[10] J. Zhang, Xuefei Ma, G. Qiao, C. Wang, A full-duplex based protocol for underwater acoustic communication networks, in: 2013 OCEANS - San Diego, 1–6, doi:10.23919/OCEANS.2013.6741129, 2013.

[11] L. Shen, B. Henson, Y. Zakharov, P. Mitchell, Digital self-interference cancellation for full-duplex underwater acoustic systems, IEEE Transactions on Circuits and Systems II: Express Briefs 67 (1) (2019) 192–196, doi:10.1109/TCSII.2019.2904391.

[12] L. Li, A. Song, L. J. Cimini, X. Xia, C. Shen, Interference cancellation in in-band full-duplex underwater acoustic systems, in: OCEANS 2015-MTS/IEEE Washington, 1–6, doi:10.23919/OCEANS.2015.7404411, 2015.

[13] G. Qiao, S. Gan, S. Liu, Q. Song, Self-interference channel estimation algorithm based on maximum-likelihood estimator in in-band full-duplex underwater acoustic communication system, IEEE Access 6 (2018) 62324–62334, doi:10.1109/ACCESS.2018.2875916.

[14] G. Qiao, S. Gan, S. Liu, L. Ma, Z. Sun, Digital self-interference cancellation for asynchronous in-band full-duplex underwater acoustic communication, Sensors 18 (6) (2018) 1700–1716, doi:10.3390/s18061700.

[15] L. Zhang, J. Huang, C. Tang, LUT based self interference cancellation (L-SIC) in bidirectional relaying underwater acoustic communication system, in: 2015 IEEE International Conference on Signal Processing, Communications and Computing (ICSPCC), 1–5, doi:10.1109/ICSPCC.2015.7338972, 2015.

[16] F. Qu, H. Yang, G. Yu, L. Yang, In-Band Full-Duplex Communications for Underwater Acoustic Networks, IEEE Network 31 (5) (2017) 59–65, doi:10.1109/MNET.2017.1600267.

[17] C. T. Healy, B. A. Jebur, C. C. Tsimenidis, J. Neasham, J. Chambers, Experimental Measurements and Analysis of In-Band Full-Duplex Interference for Underwater Acoustic Communication Systems, in: OCEANS 2019 - Marseille, 1–5, doi:10.1109/OCEANSE.2019.8867454, 2019.

[18] J. Pires, M. Colombo, J. Gallardo, C. De Maziani, R. Alcoleas, Vertical Underwater Acoustic Channel Model in Sensor Networks for Coastal Monitoring, IEEE Latin America Transactions 11 (1) (2013) 382–388, doi:10.1109/TLA.2013.6502834.

[19] B. Chun, E. Jeong, J. Joung, Y. Oh, Y. Lee, Pre-nulling for self-interference suppression in full-duplex relays, in: Proceedings: APSIPA ASC 2009: Asia-Pacific Signal and Information Processing Association, 2009 Annual Summit and Conference, 91–97, 2009.

[20] T. Riihonen, S. Werner, R. Wichman, E. B. Zacarias, On the feasibility of full-duplex relaying in the presence of loop interference, in: 2009 IEEE 10th Workshop on Signal Processing Advances in Wireless Communications, 275–279, doi:10.1109/SPAWC.2009.5161790, 2009.

[21] G. Maze, Acoustic scattering from submerged cylinders. MIIR Im/Re: Experimental and theoretical study, The Journal of the Acoustical Society of America 89 (6) (1991) 2559–2566, doi:10.1121/1.400684.

[22] T. Riihonen, R. Wichman, Analog and digital self-interference cancellation in full-duplex MIMO-OFDM transceivers with limited resolution in A/D conversion, in: 2012 Conference Record of the Forty Sixth Asilomar Conference on Signals, Systems and Computers (ASILOMAR), 45–49, doi:10.1109/ACSSC.2012.6488955, 2012.

[23] Y. Liu, X. Quan, W. Pan, Y. Tang, Digitally assisted analog interference cancellation for in-band full-duplex radios, IEEE Communications Letters 21 (5) (2017) 1079–1082, doi:10.1109/LCOMM.2017.2652444.

[24] P. Filippi, Theoretical acoustics and numerical techniques, vol. 277, Springer, 1983.

[25] P. M. Morse, K. U. Ingard, Theoretical acoustics, Princeton university press, 1986.

[26] R. W. Pryor, Multiphysics modeling using COMSOL®: a first principles approach, Jones & Bartlett Publishers, 2009.

[27] R. Courant, K. Friedrichs, H. Lewy, On the partial difference equations of mathematical physics, IBM Journal of Research and Development 11 (2) (1967) 215–234, doi:10.1147/rd.112.0215.

[28] D. Alleyne, P. Cawley, A two-dimensional Fourier transform method for the measurement of propagating multimode signals, The Journal of the Acoustical Society of America 89 (3) (1991) 1159–1168, doi:10.1121/1.400530.

[29] P. Qarabaqi, M. Stojanovic, Statistical characterization and computationally efficient modeling of a class of underwater acoustic communication channels, IEEE Journal of Oceanic Engineering 38 (4) (2013) 701–717, doi:10.1109/JOE.2013.2278787.

[30] L. M. Brekhovskikh, Y. P. Lysanov, R. T. Beyer, Fundamentals of ocean acoustics, Acoustical Society of America, 1991.

[31] F. B. Jensen, W. A. Kuperman, M. B. Porter, H. Schmidt, Computational ocean acoustics, Springer Science & Business Media, 2011.

[32] B. Barkat, B. Boashash, Design of higher order polynomial Wigner-Ville distributions, IEEE Transactions on Signal Processing 47 (9) (1999) 2608–2611, doi:10.1109/78.782225.